Energy Conversion and Management: X 20 (2023) 100428

Contents lists available at ScienceDirect

Energy Conversion and Management: X

journal homepage: www.sciencedirect.com/journal/energy-conversion-and-management-x

Experimental and theoretical analysis of a micro-cogenerative solar ORC-based unit equipped with a variable speed sliding rotary vane expander

Fabio Fatigati *, Diego Vittorini, Marco Di Bartolomeo, Roberto Cipollone

Department of Industrial and Information Engineering and Economics, University of L'Aquila, Piazzale Ernesto Pontieri, Monteluco di Roio, 67100 L'Aquila, Italy

ARTICLE INFO

Keywords:
Solar ORC-based power unit
Sliding rotary vane expander
ORC control
Domestic micro-cogenerative application
Model-based analysis

ABSTRACT

A promising solution for the Combined Heat and Power (CHP) micro production is certainly represented by Organic Rankine Cycle (ORC)-based power units. In the domestic appliances with electrical power range of the units below 1 kW, the reduced dimensions of the components represent a critical aspect as well as the need to guarantee a high reliability. When the hot source is represented by solar energy, the optimization of the electricity production keeping insured the thermal energy availability represents an aspect which invites to a proper management of the unit. Solar-based ORC-recovery units frequently work in off-design conditions due to the variability of the hot source and to the Domestic Hot Water (DHW) requirements. For this reason, the design and the selection of the components should be carefully performed. The expander is commonly retained the key component of the unit being the one that mainly affects the behaviour. For the mentioned power ranges, the volumetric expander is the best technological option and, among those available, Sliding Rotary Vane Expander (SVRE) are gaining a sensible interest. At off design conditions, according to permeability theory, the expander intake pressure linearly varies with mass flow rate of the Working Fluid (WF) which is the most suitable and easiest parameter to be changed. This modifies the performances of the unit, both from a thermodynamic and technological point of view. In this paper, the speed variation of the expander is considered as control parameter to restore design expander intake pressure. In order to assess a strategy for the speed variation of the expander, in this paper a comprehensive model of the SVRE is presented when it operates in a solar-driven ORC-based unit. The model is physically based and recovers and widens the permeability theory developed by the authors in previous works. An experimental ORC-based unit was fully instrumented and operated, coupled with a reservoir, usually present when flat plate solar collectors are used, which store the thermal energy which fulfils thermal energy requests and feeds the generating unit. The model was widely validated with the experimental data properly conceived for the purpose. In the unit the expander speed was varied and, thanks to the permeability theory, the relationships between WF flowrate variations, inlet expander pressure and expander speed variation were investigated. The potentiality of a control strategy of the expander revolution speed of the expander was fixed as well as a deeper understanding of the SVRE behaviour and relationships between operating variables. In particular, it was observed that varying the speed from 1000 RPM up to 2000 RPM, the expander behaviour was optimized ensuring proper working condition matching with a (30–100 g/s) flowrate range.

1. Introduction

Primary energy demand is rapidly increasing in recent years due to the growing world population and higher living standards. This aspect, in conjunction with an energy mix still largely dominated by fossil sources [1], contributes to higher greenhouse gas emissions and atmospheric CO_2 increase. Among the different sectors, in 2020 buildings accounts the 27% of total energy and process related direct and indirect CO_2 emissions, [2]. Indeed, the residential sector is responsible for over 20% of the World's natural gas demand, and despite a contraction during the pandemic event a rebound is observed after 2021, [3]. The troubled gas events that today characterize gas availability is an additional reason to boost the development of technological solutions that reduce consumption, by maximizing contributions from renewable sources.

* Corresponding author.
E-mail address: fabio.fatigati@univaq.it (F. Fatigati).

https://doi.org/10.1016/j.ecmx.2023.100428
Received 22 February 2023; Received in revised form 26 June 2023; Accepted 21 July 2023
Available online 22 July 2023

Nomenclature

Symbols

A	cross sectional flow area [mm^2], [m^2]
A_s	cross sectional flow area [mm^2], [m^2]
C_d	pressure drop coefficient
C_f	Fanning friction factor
D_{eq}	equivalent diameter [mm], [m]
dx	discretization length [mm]
dp	pressure differential across dx [bar], [Pa]
dV_i	infinitesimal increase of i-chamber volume [m^3]
e	total specific internal energy [kJ/kg]
F	Force [N]
f	friction factor
fluid	working fluid
H	total specific enthalpy [J/kg]
h	enthalpy [J/kg]
m	mass of the volume [kg]
$\dot{m}$	mass flow rate [kg/s]
p	pressure [Pa],[bar]
N_v	number of vanes
K_p	pressure loss coefficienct
L	leakage path characteristic length [m]-[mm]
R	specific gas constant [J/(kg·K)]
r_v	instantaneous distance between blade tip and rotor centre [m]-[mm]
T	Temperature [°C], [K]
t_{cycle}	time of a complete cycle [s]
V_w	peripheral blade tip speed [m/s]
u	velocity at boundary [m/s]
V	volume [m^3]-[L]
wall	wall
Z	compressibility factor

Subscripts

c	centrifugal force
exp	expander
i	internal pressure i-chamber
in	inlet
int	intake
is	isentropic
ind	indicated power
Leak	leakages
Losses	power losses
mech	expander mechanical power
N_{ch}	chambers number
o	outlet
p	pressure force
static	static pressure
total	total pressure
Th	theoretical
Wf	working fluid

Greek letters

α	permeability [kg/(MPa·s)]
Δp	pressure difference [bar]
δ	leakage clearance gap [m]-[μ]
μ	dynamic viscosity [Pa·s]
ρ	density
ω	expander speed [rpm], [rps], [rad/s]

Acronyms

ORC	Organic Rankine Cycle
HRVG	Heat Recovery Vapor Generator
SVRE	Sliding Rotary Vane Expander
WF	Working fluid

To overcome this issue, solar thermal collectors have been widely adopted to provide thermal energy and (DHW) needs [4] with a total installed capacity of 472 GW_{th} worldwide (data referred to 2017). This technology has been proven to be particularly efficient in highly radiated areas [5], being considered also for aggregated consumptions as it happens for district heating systems to significantly reduce natural gas demand [6,7].

The main drawback of this technology derives from the variable nature of the solar source which determines fluctuations of the produced thermal power not always time-aligned with the thermal needs. Several systems have been studied in scientific literature to limit this effect. In [8] Visa et al. experimentally assessed the performances of vertically installed solar thermal collectors on a facade of a building to improve the coverage factor at the expense of the produced specific thermal energy. In [9] a similar technology has been considered in three different climatic scenarios for the production of Domestic Hot Water (DHW) showing satisfactory results. Dehghan et al. [10] found that a simple solar system in conjunction with phase change materials and electric heaters can provide sufficient thermal energy also during winter in Norway taking advantage of thermal storage. On the other hand, in [11] a life cycle assessment of this technology in hotel buildings proved that biomass auxiliary boilers are the best choice in terms of environmental performance. The control strategy of these systems plays a crucial role in the fulfilment of thermal energy needs and received a significant interest in literature. In [12] the impact of control strategy of the solar collector on the performance of a building integrated solar heating system was assessed through dynamic system simulation. Results show that the storage volume is minimized through the application of low flow controller with a constant nominal flow rate equal to 12.5 L/hm^2. In [13] optimized control strategy for the Drake Landing Solar Community in Okotoks (Alberta, Canada) were developed. Control strategies are based on the application of model predictive control concepts. Results show how updating the supervisory control strategies ensures to reduce by 5% primary energy consumption. The results reported in [14] shows the adoption of control strategies were significant for improving the heat collection performance of solar receiver.

A way to improve the flexibility of the solar energy recovery is to convert it into electrical energy. Among the different available technologies, power units based on Organic Rankine Cycles (ORC) represent a viable solution to exploit medium and low temperature heat sources. Its potential is assessed in different waste heat recovery applications like waste forest biomass [15], wastewater treatment systems [16], geothermal energy [17] and Internal Combustion Engines [18]. Although these cited fields are usually characterized by higher temperature levels, several studies investigated the potential of this technology when the hot source has low temperature value (100 °C) as it happens with thermal mediums heated by solar energy. Hossin et al. [19] analysed a small-scale solar ORC-based unit using evacuated flat tube collectors and a simple thermodynamic layout of the cycle. The results show that an efficiency of 6.75% is achievable for a hot water inlet temperature of 120 °C. Gilani et al. [20] investigated a similar solar system paired with a recuperative ORC-bases unit to assess the possibility to supply electric energy for the conditioning in a two-story office building located in Cyprus. The analysis found that 97 % of the energy demand of the refrigeration system can be supplied by the solar recovery, leading to a saving of 2000 USD per year. In [21] an exergy-enegy analysis was carried out for a solar-driven trigeneration system employing parabolic solar collector. Results shows as an exergy

efficiency of 21% and an electrical-exergy efficiency of 17.5% can be achieved. Moreover, suitable parameter to control the unit are the variation of the solar fields outlet temperature and the ORC condensation temperature.

In [22] the integration of a 1 kW ORC based power unit with a residential thermal installation was assessed. It was found a high dependence of viability of the retrofit with the electricity prices due to the variability of solar radiation and the demand of DHW affecting respectively the outlet temperature level of the collector water and the input water to the ORC evaporator.

The implementation of a suitable control strategy in ORC-based power units relies on the number of control parameters. The regulation of the pump speed allows to control the mass flow rate of working fluid circulating inside the plant. Such parameters is varied to follows the availability of thermal power of hot source. Other parameters are the mass flow rate of the hot and cold source. An important degree of freedom in the control system is certainly the regulation of expander speed. In [23] the optimal design and control strategy of a solar driven ORC based power unit was assessed. The system employs two tank sensible thermal energy storage and it was controlled acting on Heat Transfer Fluid (HTF) flow rate.

In [24] the authors conducted an exergy-based and economic analysis on a small-scale ORC-based solar unit bottoming different solar architectures providing thermal energy to the evaporator through an intermediate circuit. In addition, several locations have been considered. The maximum exergy efficiency (6.2%) is achieved with evacuated tube collectors using R245fa as the thermodynamic working fluid in Istanbul. Ancona et al. [25] developed a semi-empirical model of an ORC-based unit equipped with a piston expander bottoming a solar system with thermal storage for residential applications. The analysis found that approximately 15 % of the yearly electric energy demand can be satisfied. Furthermore, the analysis pointed out that an optimized control strategy could increase the production capability, especially at lower solar irradiation leading to better overall performances. A fast and robust control of the expander inlet pressure is the control of the expander speed [26]. As the superheating degree and expander intake pressure are strongly correlated [27], the control loop of the intake pressure should be one order of magnitude faster than the superheating controller in order to prevent interactions between the control loops, [26]. Hence, changing the expander speed allows the optimization of the expander performances at different WF flow rates [28], varying the maximum pressure of the cycle and consequently the overall performance of the unit [29]. The variation of the WF flow rate is the easiest way to exploit the possibility to vary the thermal power from the hot source which follows its variations during time.

Expanders can be divided into dynamic and volumetric machines [30] with the former more suitable for use in larger power plants for stationary applications [31] and the adoption of standard turbine allow to reduce the development and manufacturing cost, [32]. On the other hand, volumetric expanders include a wide variety of different machines [33] mostly preferred in small-scale power units because of their ease of operation, wider range of operativity and off-design better performances [34].

Among volumetric expander, sliding rotary vane machine are less used with respect to other technology such as scroll and twin screw and piston for larger application. Moreover, for this kind of device there are few integrated and experimental analysis about the impact of expander speed variation on the performance of SVRE and of solar micro-ORC based power unit (power $<$ 1 kW) in which the expander are introduced. Therefore, to fill this gap, in this study a wide experimental activity was developed on the variable speed SVRE. The experimental database allows to validate a detailed model of SVRE build according an integrated zero and mono dimensional approach. The model approach was the same followed by author for a larger SVRE employed for Internal Combustion Engine Waste Heat Recovery application. Nevertheless, in this case the expander present a different port structure (radial intake and exhaust port) and lower dimensions. Moreover, a novelty with respect the previous model [29] is the model was experimentally validated considering multiple expander speeds SVRE was introduced inside an ORC test bench to be integrated with flat solar thermal collector in residential application. In laboratory scale, the hot source is represented by hot water inside a reservoir usually operated with the flat panels. The temperature of the water inside the reservoir is approximately close to 100 °C as it is in real applications. Previously, a similar layout was used to understand the influence of the expander type on the performance of the whole unit [35]. In that case, the main objective was to experimentally assess the performance of the unit at different rotational speeds with the final aim to optimize the electric power production when the operating conditions of the recovery unit are far from the design one. As already observed, the off design of the recovery unit is a usual situation considering that the temperature of the water inside the reservoir continuously changing for the thermal demand by the users which is substantially unpredictable. The solar energy restoring, as well, is changing during time, here simulated modulating the electrical energy delivered by the resistances.

The management of the speed of revolution of a SVRE in order to maximizes the electricity production keeping the same frequency of the electricity is a new concept in literature, mainly when the recovery unit is characterized by a reduced power produced (0.5–1 kW). In the specific application for a domestic CHP unit, the maximization of the electricity production is particularly suitable for the fulfilment of the daily-varying electric needs which with a small electrical battery can cover completely the requests. The study is based on an updated modelling of the SVRE which supported a model-based control strategy.

2. Material and methods

2.1. Experimental layout

A fully instrumented ORC-based power unit was developed (Fig. 1) simulating the solar power with two electric resistances (12 kW each), which provide the thermal power to 135L of water stored in a pressurized tank (p). The hot water flows in a plate heat exchanger (o), exchanging heat with the working fluid (R245fa). The superheating degree has been fixed at 10 °C in design operating conditions.

The working fluid circulation was ensured by a diaphragm pump (c) (whose volumetric capability is equal to 6.1 cm^3) actuated by an electric motor. Thanks to a dedicated inverter, its revolution speed can be varied to regulate the mass flow rate of the working fluid to follow the variation of the hot source thermal energy in the most efficient way.

Downstream the Heat Recovery Vapor Generator (HRVG) (e), the superheated working fluid enters the Sliding Rotary Volumetric Expander (SVRE) (f) producing mechanical power which is converted into electric form through an electric generator (l). The working fluid exiting the expander flows in a recuperator heat exchanger (g), thus preheating the working fluid entering the HRVG.

The mechanical connection between the expander and the electric generator is worth mentioning. The expander shaft was coupled with the electric generator (l) through a torque meter (m) and flexible joints (o) (Fig. 2). In this way, the measurement of mechanical power can be provided. Moreover, a regenerative inverter was adopted to vary the expander revolution speed. This feature is a fundamental peculiarity of the ORC plant, which ensures widening the regulation degree of freedom of the unit. Indeed, the pump speed defines the mass flow rate circulating inside the plant. In contrast, the expander speed sets the plant's permeability and maximum pressure for a given flow rate.

If the expander speed is fixed, the plant permeability remains constant and the maximum pressure follows a univocal linear increase with mass flow rate. Therefore, the present experimental campaign provides an experimental demonstration of the permeability theory. The working fluid leaving the expander enters the hot side of a regenerator (g) to preheat the working fluid at the cold side sent by the pump (c). Once the

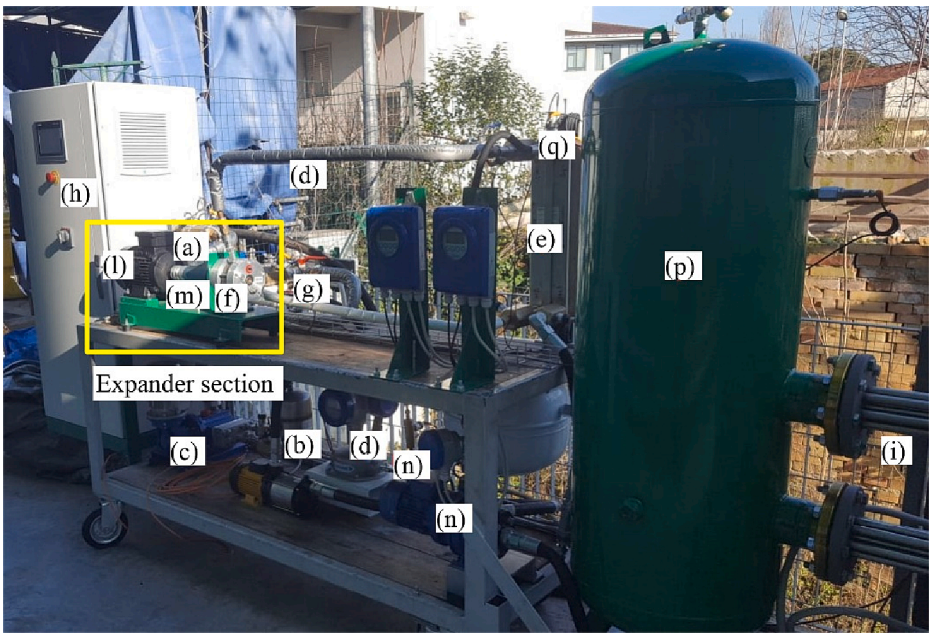

Fig. 1. Solar ORC-based power unit. (a) condenser; (b) 3L plenum; (c) pump; (d) Coriolis R245fa flow meter; (e) Heat Recovery Vapor Generator HRVG; (f) Sliding Rotary Vane Expander SVRE; (g) recuperator; (h) Control Unit; (i) 12 kW electric resistance; (l) electric generator; (m) torque-meter; (n) hot water pump; (p) hot water tank; (q) temperature and pressure transducers.

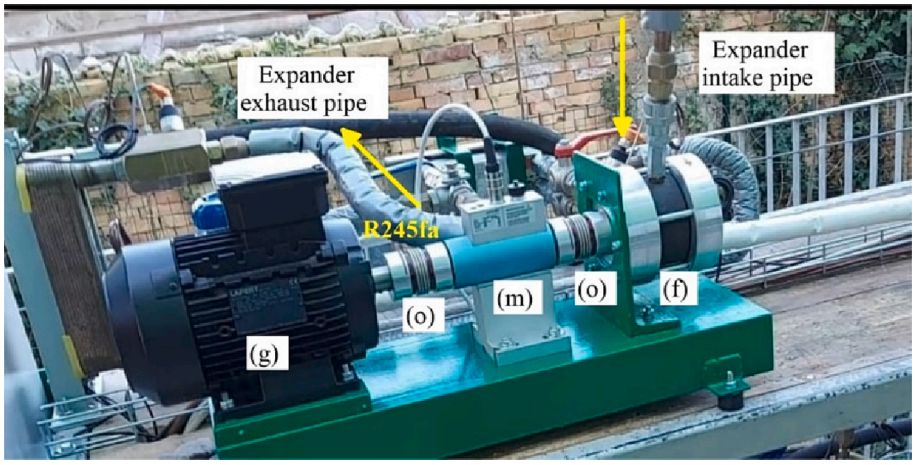

Fig. 2. The connection between expander, torque-meter, flexible joints and electric generator; (f) SVRE expander; (o) flexible joints; (m) torquemeter.

working fluid leaves the regenerator hot side, it is gathered in a 3 Liters plenum, introduced to dump the flow rate fluctuations. Subsequently, it flows into a plate heat exchanger, where it condenses.

The test bench is fully instrumented to assess all the operating quantities characterizing the unit. A Coriolis (d) flow meter was adopted to measure the mass flow rate of R245fa, while the flow rate of hot and cooling water was measured with magnetic flow meters at the HRVG and the condenser. Pressures and temperatures were assessed upstream and downstream of each component and the pump power was measured through a wattmeter. Concerning the expander, the torque meter (m) allows the evaluation of the mechanical power via torque and revolution speed measurement. Table 1 reports the uncertainty of the measurements of each instrument.

Table 1
Measurement uncertainty.

Variable	Sensor Type	Measurement uncertainty
Temperature	T-type Thermocouple	± 0.75 °C
Pressure	IFM electronics Pressure transducers	± 1.5% of full-scale
Mass flow rate (R245fa)	Coriolis Flow meter- Optimass 5300 Khrone™	± 0.15% measured value
Mass flow rate (water)	Magnetic Flowmeter- Optiflux 4000 Khrone™	± 0.5% measured value
Power	Wattmeter PCE™	± 1% measured value
Torque	Torque-meter Kistler™ 4503B	± 0.2 Nm
Revolution speed	Torque-meter	± 1 rpm

2.2. Experimental procedure and uncertainty analysis

The SVRE was tested in steady state conditions over a wide operating range characterized by a flow rate varying between 30 g/s and 80 g/s

and an expander revolution speed ranging from 1250 RPM up to 1750 RPM. The adopted procedure was the following:

1. The acquisition starts after the ORC-based unit reaches the steady state conditions at the fixed working point
2. The data-acquisition was performed thanks to a customized software developed in the Siemens Simatic HMI™. The software allows to collect the data with a sampling time of 2 s and to manage the main operating quantities such as the working fluid mass flow rate;

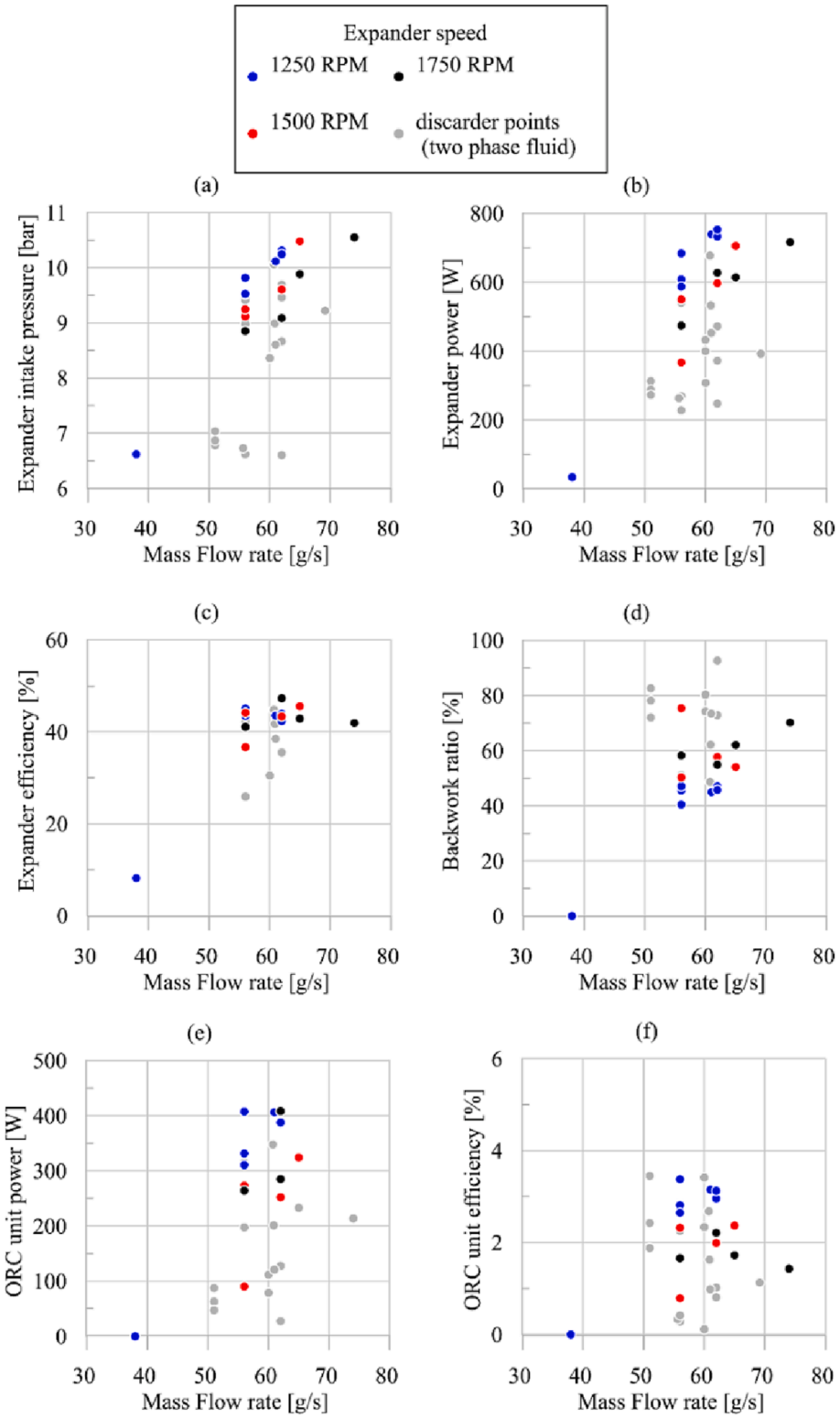

Fig. 3. Selected and discarded data in terms of expander intake pressure (a), power (b), efficiency (c), backwork ratio (d), ORC unit power (e) and ORC unit efficiency (f) as function of mass flow rate.

3. The uncertainty analysis was carried out following the approach of [36] where the uncertainty U_y of a quantity y as function of measured variables $x_1,x_2,..x_i,...x_n$ are evaluated as in Eq. (1):

$$U_y = \sqrt{\sum_{i=1}^{n} \left(\frac{\partial y}{\partial x_i}\right)^2 U_{x_i}^{\ 2}} \tag{1}$$

Where U_{xi} is the uncertainty of the i-variables. In Table 1 the uncertainty of the measurements of each measurement is reported.

The data was then post-processed, averaged and filtered. In particular, only the data corresponding with a superheating degree comprised between 2 and 10 °C were collected. Superheating degree ΔT_{SH} was defined as in (2), where $T_{exp,in}$, T_{sat} and $p_{exp,in}$ are respectively the expander intake temperature and pressure and the saturation temperature in correspondence of $p_{exp,in}$.

$$\Delta T_{SH} = T_{exp,in} - T_{sat}\left(p_{exp,in}\right) \tag{2}$$

Hence, the data corresponding to two-phase working fluid conditions are discarded as it can be seen in Fig. 3. In it, the discarded values of expander intake pressure (a), expander power (b) and efficiency (c), Back-work ratio (d), ORC-based power (e) and efficiency (f) have been also reported. It is interesting to observe how despite the SVRE elaborates a two-phase working fluid, it is still able to produce useful power. Nevertheless, the performances are significantly penalized as it can be seen by the lower expander and unit efficiencies referred to the discarded points.

In order to assure a high rate of the accuracy, the heat exchangers, the connecting pipe, the expander and pumps are insulated in order to avoid thermal losses which could affect the measurement reliability. Moreover, thermocouple and pressure sensors are located close each other on *T* connectors. Finally, the alignment of expander, torque-meter and electric generator are carefully verified.

2.3. SVRE theoretical model

The novelty of the validation is that it accounts for the expander speed variation. Indeed, authors previous model developed with the same approach was validated on a constant rotational speed. Speed variation modifies many processes (most important are vane filling and emptying which are unsteady processes which behave as boundary conditions of the connecting pipes) and, due to this, the model accuracy was improved. The experimental agreement with theoretical data confirms a wider validity of the model and an increased capability to predict phenomena. Hence, to the author best knowledge, a so deep analysis on a Sliding Rotary Vane Expander for micro ORC-based application are still not available in literature.

The expander speed variation was realized introducing a regenerative inverter on the electric generator entrained by the expander. This aspect also represents a novel contribution to the sector. Usually, the generator fixes a constant speed of revolution due to the frequency of the grid to which it is connected. The size of the expander, as well, falls in that class which can be defined mini or micro, being the rated power equal to 750 W. This power level is not so frequent in literature.

The experimental data ensured to validate a comprehensive model of SVRE when the expander revolution speed varies. This model has never been validated before against experimental data referred to revolution speed variation which introduces variable phenomena. Despite the novelties introduced by the experimental validation and the adaptation of the model to a smaller expander with a different ports architecture, the model structure is the similar to that adopted by the authors for the characterization of a larger size SVRE in [29].

The model reported in Fig. 4 was developed adapting to the new machine the approach followed for a higher capacity SVRE expander [35].

The approach follows a mono and zero-dimensional thermo-fluid-dynamic analysis and it was developed in GT-Suite™. The mono-dimensional approach was adopted to reproduce the dynamic process taking place inside the intake (b) and exhaust pipes (d). It involves the discretization of intake and exhaust pipes into sub-elements, solving for each of them the Navier-Stokes equation systems (3).

$$\frac{dm}{dt} = \sum_{boundaries} \dot{m} \tag{3.1}$$

$$\frac{d\dot{m}}{dt} = \frac{dpA + \sum_{bound}(\dot{m}u) - 4C_f \frac{pu|u|}{2}\frac{dxA}{D_{eq}} - K_p\left(\frac{pu|u|}{2}\right)A}{dx} \tag{3.2}$$

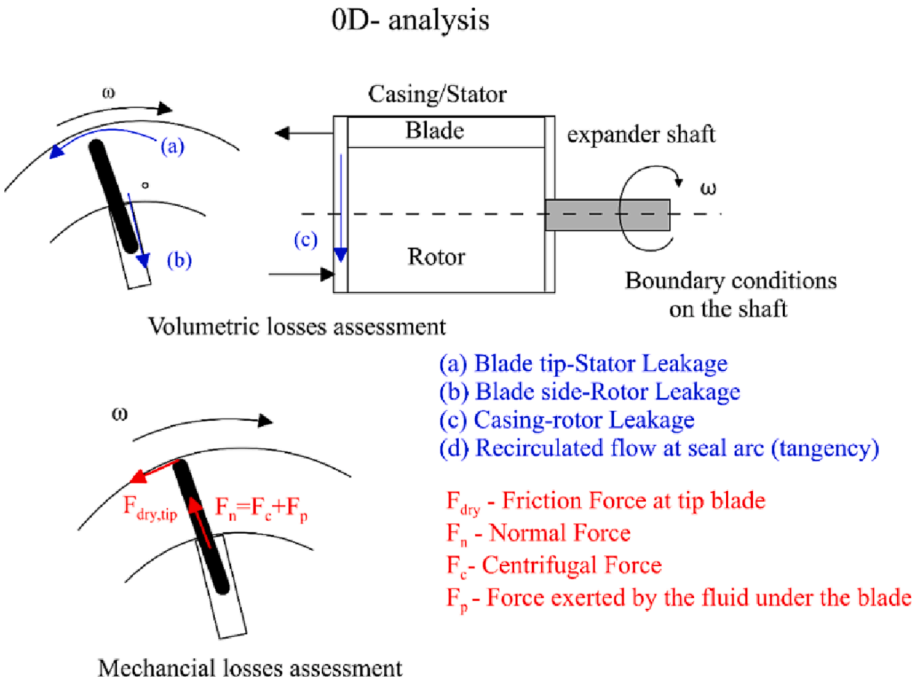

Fig. 4. Scheme of 0D-analysis.

$$\frac{d(me)}{dt} = -\rho\frac{dV}{dt}\sum_{boundaries}(\dot{m}H) - hA_s\left(T_{fluid} - T_{wall}\right) \tag{3.3}$$

Equations are integrated through an explicit solver. It is important to notice that scalar variables such as pressure, enthalpy, etc… are assumed to be uniform over each volume while vector variables (mass flowrates) are calculated for each boundary separating the sub-volume in which an element is discretized.

The inlet and outlet boundary conditions are considered as infinite capacity plenums, represented by total conditions imposed by the HRVG at its outlet and a static pressure at the condenser fixed by the temperature of the cooling fluid (tap water). In this way it was possible to extract the expander from the whole circuit considering it separately.

The right boundary conditions of the inlet pipe and the left one of the outlet pipes are represented by the expander chambers which fill or empty. They have been simulated by plenums having finite capacity whose total conditions change during time according to flowrate entering or living them and to the volume variation due to the rotation. Expander rotational speed can be imposed through the element (m) which is directly linked to the expander shaft sub-model.

In Fig. 4, the 0-D analysis was schematized in the assessment of volumetric and mechanical losses. The expander speed, which is externally imposed through the regenerative inverted.

The volumetric losses are given by the difference between the experimental and theoretical volumetric flow rate. These parameters assume the same value only if leakage losses are absent. The theoretical flow rate is given by the product of the working fluid density ρ, the expander chamber intake volume V_{int}, the number of vanes N_v and the revolution speed, Eq. (4):

$$\dot{m}_{wf} = \dot{m}_{th} + \dot{m}_{leak} = \rho N_v V_{int}\omega + \dot{m}_{leak} \tag{4}$$

Therefore, the ratio between theoretical and experimental flow rates represents the volumetric efficiency.

The model evaluates the leakage losses occurring in the gaps between the blade tip (a) and the stator inner surface, the blade sides and rotor slots (b) and between the rotor face and the machine casing (c).

The first two leakages are evaluated according to the Poiseuille-Couette approach (5) whereas the latter is evaluated according to the equivalent diameter approach (6). This method assumes that leakages take place across an equivalent orifice whose area is equal to that of the gap between the rotor faces and the machine casing.

$$\dot{m}_{leak,i} = \rho\delta W\left(\frac{\delta^2\Delta p}{12\mu L} + \frac{1}{2}V_w\right) \tag{5}$$

$$\dot{m}_{leak,i} = C_d\frac{\pi D_{eq}^2}{4}\rho\sqrt{2\frac{\left(p_{1,total} - p_{2,static}\right)}{\rho}} \tag{6}$$

In Fig. 4, the procedure to evaluate the mechanical power losses is depicted. The mechanical losses are mainly caused by the dry contact between the blade tips and the stator inner surface. Thus, the friction power losses depend on the normal force that the blade exerts on the stator inner surface (7). This in turn depends on the centrifugal force and the pressure exerted by the working fluid filling the gap under the blades when they outstand towards the stator inner surface. The mechanical losses are evaluated thanks to the subroutine (l).

$$P_{losses} = fN_v\left(F_c + F_p\right)r_v\omega \tag{7}$$

Such relation was implemented inside subroutine (l) which ensures to represents all the dry and viscous friction phenomena. Indeed, (l) subroutine allows to consider the effects of viscous friction on bearings, and between the rotor face and casing, blades tips and rotor slot, blades tips and stator inner surface. Nevertheless, the only dry friction losses between blade tips and stator inner surface has been considered, representing almost the 95% of the whole power losses, [29].

Subtracting the power losses to the indicated power given by the area of the indicated diagram of the chambers (8) the expander power available on the shaft is obtained (9).

$$P_{ind} = \frac{\sum_{i=1}^{N_v}\oint p_i dV_i}{t_{cycle}} \tag{8}$$

$$\mathrm{P_{mech}} = \mathrm{P_{ind}} - \mathrm{P_{losses}} \tag{9}$$

Concerning the expander global efficiency, it is given by the ratio between the mechanical power and the one corresponding to an adiabatic isentropic transformation (10).

$$\eta_{\exp} = \frac{P_{mech}}{\dot{m}_{WF}\left(h_{\exp,in} - h_{\exp,out}\right)} \tag{10}$$

The boundary conditions are set through the intake (a) and exhaust plenum (e). These are represented by mass flow rate and inlet temperature in (a) -total temperature condition- and exhaust pressure in (e). In Fig. 4 a scheme was developed to summarize the approach followed. The model was experimentally validated thanks to a wide set of experimental data which included the speed variation of the expander, so widening its validity in a manner never considered untill now.

Hence, The model of the SVRE is physically based and the validation phase ensures to calibrate some parameters which cannot be stated in an analytic manner. For instance, the clearance gap between blades tip and stator inner surface was experimentally identified also considering that it depends on operating conditions. Nevertheless, its identification is univocal as there is only one values which ensures that the expander intake pressure and expander power are properly predicted with respect to the experimental data. Moreover, thanks to the wide calibration phase the trend of this parameter with the main operating quantities (mass flow rate, operating speed) is identified ensuring to widen their prediction outside the experimented working range.

3. Results

3.1. Experimental results and model validation

The experimental analysis was focused on the effect of the revolution speed variation on the expander performance. The expander is commonly retained as the critical component of the whole unit since its behavior affects the operating conditions and the performance of the whole unit. If a volumetric expander is employed, it can be seen as a revolving valve, influencing the maximum pressure of the unit with its permeability. The permeability is defined as the attitude of the expander to be crossed by the working fluid. The lower the permeability, the higher the maximum plant pressure. This parameter can be varied to set the maximum plant pressure since the permeability depends on the expander speed [23]. Furthermore, the expander performances are particularly sensitive to revolution speed variation and its impact should be carefully considered.

To experimentally analyse these aspects, a dedicated experimental campaign was carried out considering 3 expander speeds (1250 RPM, 1500 RPM, and 1750 RPM). The results were reported in terms of expander intake pressure (Fig. 5(a)), power (Fig. 5(b)), and global efficiency (Fig. 5(c)) as a function of the mass flow rate provided by the pump.

It can be seen from Fig. 5(a) that the expander intake pressure follows a different linear growth path with mass flow rate according to the expander speed. Increasing the revolution speed the slope of the linear growth diminishes due to the increase of the expander permeability. It passes from 0.08 kg/(MPa·s) when the expander rotates at 1250 RPM to 0.01 kg/(MPa·s) for a revolution speed of 1750 RPM. This means that keeping constant the mass flow rate, the higher the revolution speed the lower the expander intake pressure which, net to the pressure drop between HRVG and SVRE, coincides with the maximum plant pressure.

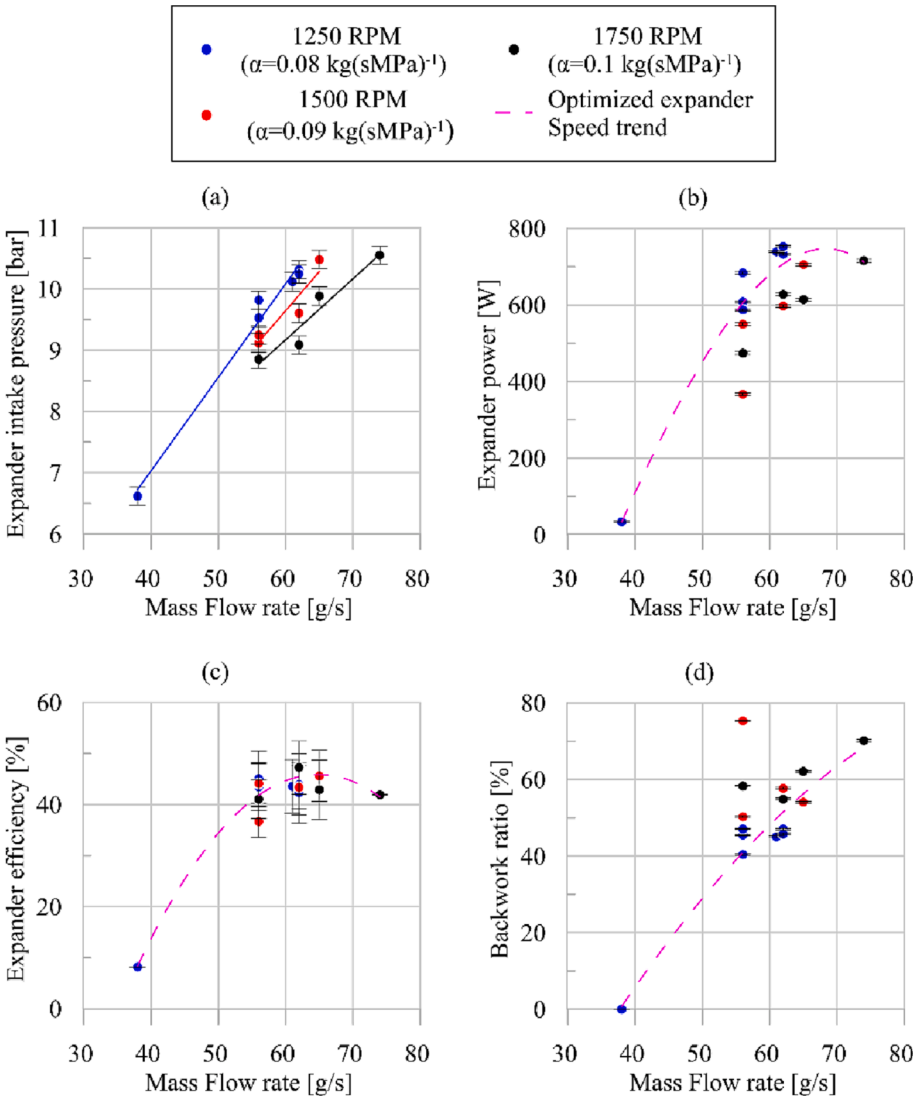

Fig. 5. Effects of revolution speed variation on Expander intake pressure (a), power (b) and efficiency (c) as a function of mass flow rate.

Considering a mass flow rate equal to 62 g/s, the expander intake pressure is equal to 10.3 bar, 9.6 bar and 9.1 bar when the expander speed is respectively equal to 1250 RPM, 1500 RPM and 1750 RPM.

The different pressure trends affect the expander power, which follows a linear growth with the mass flow rate in each case. Indeed, for mass flow rates between 38 g/s and 62 g/s, the maximum power is achieved at 1250 RPM (760 W).

It is important to notice that increasing the revolution speed, the slope of the linear growth of power with mass flow rate diminishes as can be observed in Fig. 5(b). This is a consequence of the permeability increase with expander speed increase. In fact, the higher is the expander speed, the lower is the expander intake pressure growth with mass flow rate (Fig. 5(a)). As the exhaust pressure depends by the cold source conditions and it is quite constant with mass flow rate, also the linear growth of expander pressure ratio diminishes with mass flow rate, increasing the expander speed. Anyway, the increase of expander speed allows to widen the operability because if this parameter remains fixed with mass flow rate growth, the expander intake pressure could reach very high pressure values, reducing the machines efficiency and increasing the expander cost. Hence, results mean that the revolution speed should be increased with the mass flow rate to provide the best operating conditions for the SVRE [23].

Experimental results reported in Fig. 5 are in accordance to the permeability theory, [28]. Indeed, the experimental trend confirms the theoretical relation of permeability expressed in [28]. As reported in [28], it can be obtained integrating the mass conservation (11) and the real gas behaviour relation (12).

$$\rho_{int} = \frac{\eta_{vol}\dot{m}_{wf}}{\omega_{\exp} V_{int} N_{ch}} \tag{11}$$

$$p_{int} = ZRT_{int}\rho_{int} \tag{12}$$

$$p_{int} = ZRT_{int}\frac{\eta_{vol}\dot{m}_{wf}}{\omega_{\exp} V_{int} N_{ch}} \tag{13}$$

Observing equation (13), it can be seen as once the expander speed is fixed, all the quantities reported are constant with the exception of the intake pressure and temperature and mass flow rate which is intrinsically related to the expander intake pressure. Nevertheless, it was observed [28] that for low superheating degree variations (typical of such application where superheating rarely exceeds 20 °C) its effect is negligible on expander intake pressure (and mass flow rate). Hence, eq.10 can be retained linear and the slope is equal to the reciprocal of permeability. Indeed, permeability is defined by the ratio between the mass flow rate and pressure rise and the (14):

$$\alpha = \frac{\dot{m}_{WF}}{\Delta p_{\exp}} \tag{14}$$

Therefore, Eq. (15) can be written:

$$\alpha = \frac{\dot{m}_{wf}}{\left(ZRT_{int} \frac{\eta_{vol} \dot{m}_{wf}}{\omega_{\exp} V_{int} N_{ch}} - p_{\exp,out} \right)} \tag{15}$$

However, as the exhaust pressure is quite independent from mass flow rate, permeability can express the linear relation between mass flow rate and expander intake pressure. In particular, the higher is the permeability, the lower is the expander intake pressure for a given mass flow rate. Furthermore, equation (12) puts in light the role of expander speed. Indeed, the higher is the expander speed the larger is the permeability and the lower is the slope of the curve. This demonstrates the slope reduction observed by the experimental results for expander speed increase in Fig. 5(a). The working fluid can assume a different value for a given mass flow rate and this leads to a slight variation of the permeability. Consequently, on the linear relation of pressure with mass flow rate. This explains why for a given mass flow rate, the expander intake pressure and power could be different. The reason is the superheating degree in this case which doesn't remain constant. Indeed, the higher is the superheating degree the higher is the expander intake pressure (and the power) for a given mass flow rate and, consequently, the lower is the permeability.

This aspect can be seen also from the expander efficiency point of view. As shown in Fig. 5(c), the revolution speed regulation flats the efficiency curve. In this way, the efficiency is always comprised between 0.4 and 0.45 for mass flow rate comprised between 38 g/s and 75 g/s in accordance with the best literature results, [37]. It is worth observing that the expander performance decrease at 38 g/s in terms of power and efficiency. This happens because at 38 g/s the expander intake pressure is too low for the considered revolution speed (1250 RPM). Hence, the performance in this point could improve by reducing the expander revolution speed to increase the intake pressure and consequently the pressure ratio at the expander side.

It is worth to notice how the pump power is a significant part of that produced by the expander as expressed by backwork ratio (Fig. 5(d)) defined as the ratio of pump and expander power. It reaches value up to 70 % for the upper limit mass flow rate.

Given the influence of the expander on the unit performance, the revolution speed has effects also on the ORC-based unit output power (16) and efficiency (Fig. 6). Nevertheless, the ORC-based unit net power (Fig. 6(a)) shows a maximum for a mass flow rate of 60–65 g/s. This is due to the impact of pump power which for higher mass flow rate represents almost the 70% of the expander power. As the ORC-based unit efficiency (17) is highly dependent on the power of the unit, a maximum can be observed also for the efficiency. It interesting to observe how the mass flow rate which allows to maximize the power (60 g/s) is close to that allowing to maximize the efficiency (55 g/s). Hence the mass flow rate maximizing the power can be chosen without penalizing the efficiency (Fig. 6(b)).

$$P_{ORC} = P_{exp} - P_{pmp} \tag{16}$$

$$\eta_{ORC} = \frac{P_{ORC}}{\dot{m}_{hw} c_{p,hw} \left(T_{hw,in} - T_{hw,out} \right)} \tag{17}$$

It is worth noting how varying the expander revolution speed, the efficiency is comprised between 2% and 4 % for a huge mass flow rate interval of 50–75 g/s. This can be furtherly enhanced by reducing or increasing the revolution speed at lower or greater mass flow rates.

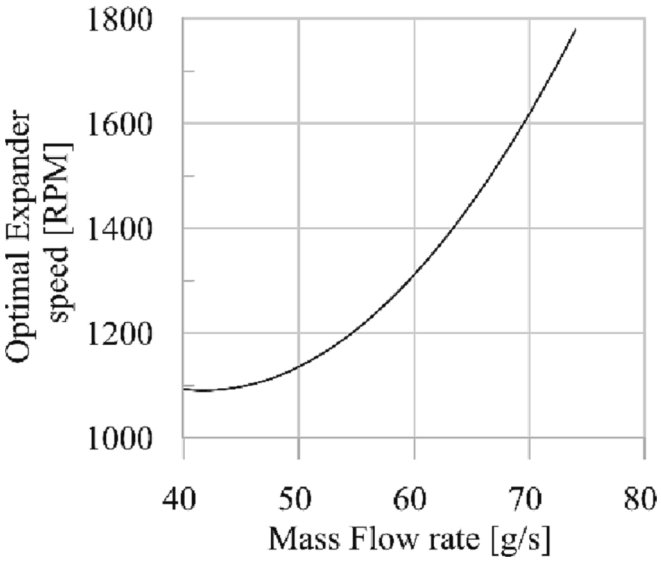

Fig. 6.1. Experimentally optimized expander speed trend allowing to maximize expander and ORC plant performance.

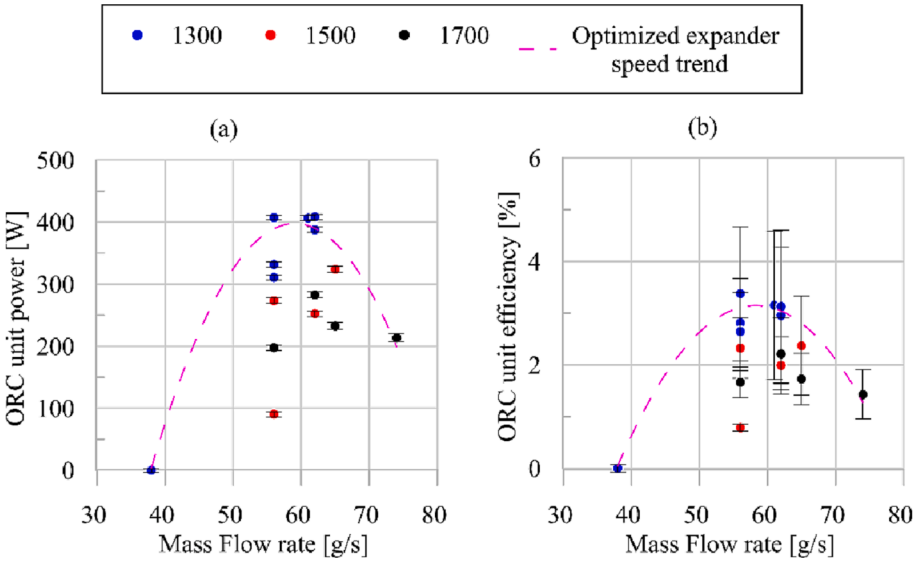

Fig. 6. Effects of revolution speed variation on ORC Net power (a) and efficiency (b) as a function of mass flow rate.

Therefore, for SVRE an optimized trend can be defined varying properly the revolution speed. Such trend (Magenta scattered lines in Fig. 5(b) and 5(c)) is achieved with a proper variation of the expander speed with working fluid mass flow rate. This law was achieved from the analysis of the experimental data. Hence, for each mass flow rate was selected the expander speed maximizing the expander power according to the experimental law reported in Fig. 6.

The trend of Fig. 6.1 was achieved selecting the revolution speed that, for each mass flow rate, allows to maximize the expander power (Fig. 5(b)). It is important to observe how the trend corresponds to fit the higher values of the expander efficiency (Fig. 5(c)) and the ORC-based power (Fig. 6(a)) and efficiency (Fig. 6(b)).

The experimental data ensured to validate the theoretical model. Intake pressure, power, expander outlet temperature and efficiency were selected as validation parameters.

Fig. 7(a) demonstrates the good agreement between experimental data and theoretical prediction. Fig. 7(a) shows how the model is capable to represent the expander intake pressure when the revolution speed varies. In this case, the maximum deviation is 6.4% whereas the Root Mean Square Error (RMSE) is 6.4%. Concerning the expander power, the model provides an accurate representation of the real values as it is demonstrated in Fig. 7(b). In this case, the maximum deviation is 8.4% and the RMSE is 2%.

Moreover, the expander outlet temperature (Fig. 7(c)) presents good accordance between experimental data and theoretical predictions. The maximum absolute deviation is equal to 5.6 °C and the average error is 2.23 °C. As a consequence of the correct representation of the considered quantities, also the global efficiency is properly evaluated by the model (Fig. 7(d)). In this case, the RMSE is equal to 2.1% whereas the maximum deviation is 7.1%.

3.2. Theoretical analysis of the impact of revolution speed on expander and plant performance

Once the model has been validated, it was used as a software platform to assess the impact of the revolution speed variation on the expander and plant performance over a wider operating range. The results were reported in maps showing expander and plant performances as a function of the mass flow rate provided by the pump and the expander speed. In Fig. 8(a) and Fig. 8(b) the ORC maximum pressure and expander pressure ratio are reported. Both parameters depend on the expander permeability in accordance with the analysis developed in [28].

Fig. 8(a) shows how the slope of the linear growth between maximum pressure and mass flow rate diminishes when expander revolution speed increases. Hence, as shown in the previous section, by changing properly the revolution speed with the mass flow rate variation (black lines in Fig. 8(a)), the maximum pressure at expander inlet can be kept close to the design value. In this way, the reduction of the revolution speed for limited mass flow rates prevents too low maximum pressures, thus ensuring appropriate working conditions of the recovery unit. On the other hand, when the WF mass flow rate grows, the expander speed increase allows to avoid the reaching of unsuitable values of maximum pressure, undermining the components' integrity and the recovery unit operation. Thus, a proper variation of the expander revolution speed according to the WF mass flow rate provides

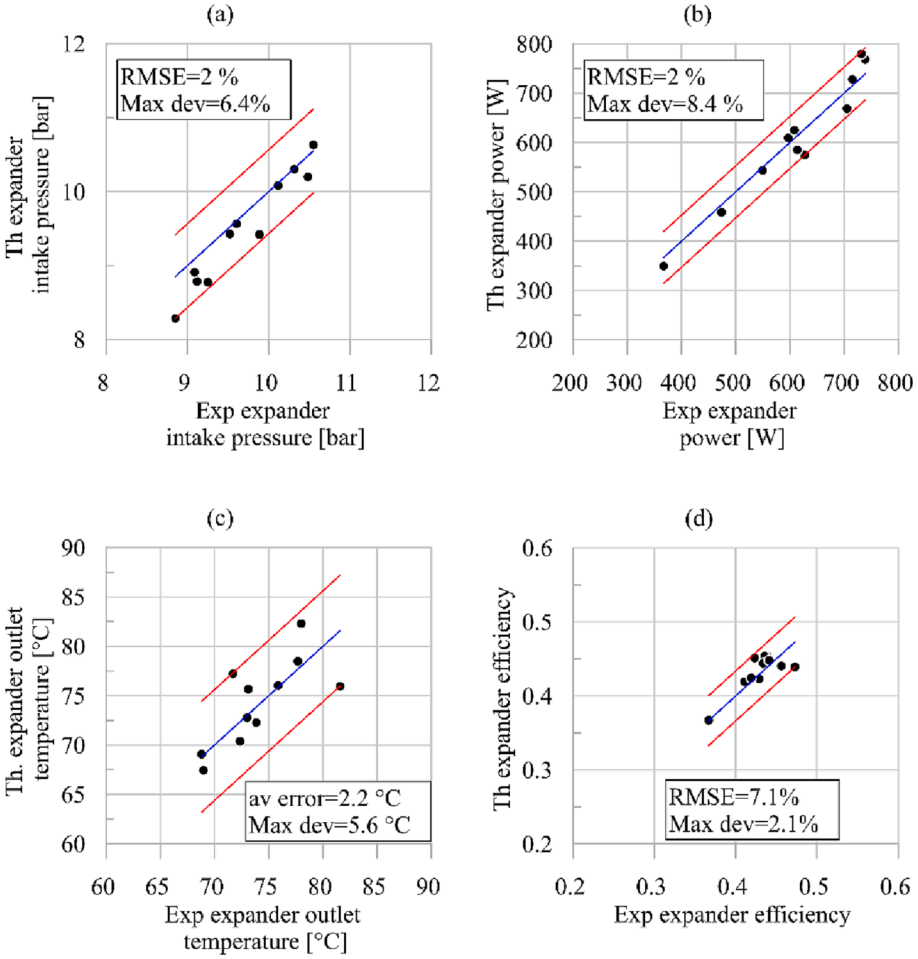

Fig. 7. Comparison between experimental and theoretical expander intake pressure (a), power (b), expander outlet temperature (c) and expander efficiency.

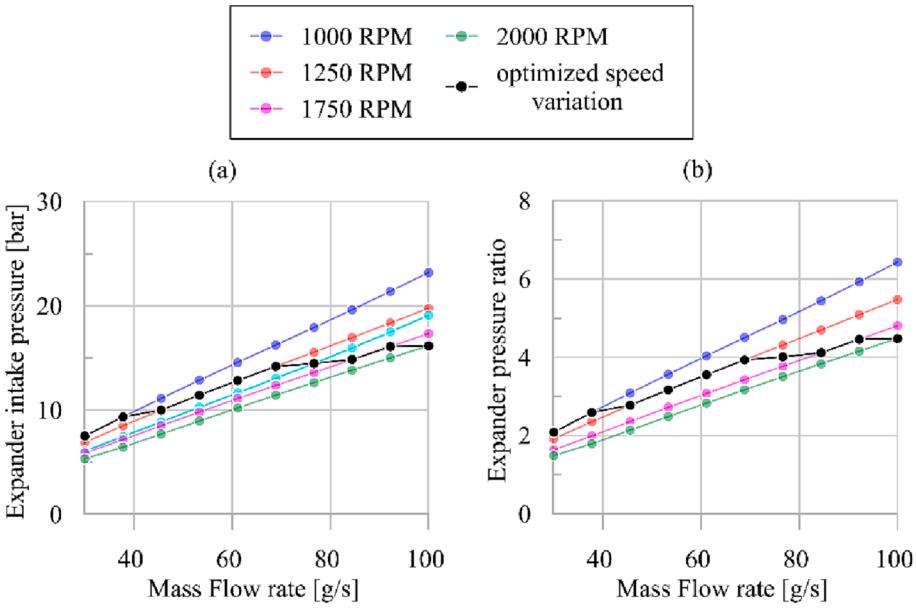

Fig. 8. Iso-contours of maximum pressure (a) and expander pressure ratio (b) as a function of the working fluid mass flow rate and speed.

that the expander pressure ratio varies in a proper interval (2–5) despite the significant operating conditions change (black lines in Fig. 8(b)). Hence, if the pressure ratio remains closer to the built-in volume ratio of the machine equal to 5, the under and over expansion phenomena can be prevented.

In the present analysis, the pressure ratio is obtained by keeping constant the expander exhaust pressure at 2.61 bar since this value depends only on the condenser condition. Anyway, if the variation of the exhaust pressure would change (according, for instance, with a different temperature of the condensing medium), the corresponding value of the expander pressure ratio can be obtained by interpolation.

Therefore, once a given optimized pressure or pressure ratio profile is defined, the reported maps (Fig. 8) can be used as a control tool to set the revolution speed that allows achieving the desired values in terms of pressure. Indeed, entering the mass flow rate value provided by the pump (which is defined according to the thermal power availability at the hot source) when the curve corresponding to the required pressure (or pressure ratio) is intersected, the expander revolution speed can be evaluated. As discussed in previous section, the expander intake pressure and pressure ratio profile are achieved properly varying the expander speed to maximize the expander power (Fig. 9(a)). From Fig. 9 (a) it can be seen how if the expander speed is kept constant, the value of expander power is lower than the one achieved varying the expander speed (black line). Despite the optimization is performed on expander power, the expander speed variation allows to achieve efficiency close to the maximum value (Fig. 9(b)). In this case also it can be seen that to the optimized line corresponds the highest efficiency for each mass flow rate. Exception is present in the range 60 g/s-100 g/s where the maximum efficiency is achieved for the case of 2000 RPM. Nevertheless, the difference is limited to few points while the advantage to vary the expander speed allows to significantly improve the efficiency for mass flow rate lower than 60 g/s.

In Fig. 9(a) and 9(b) the values of expander power and efficiency corresponding to the case in which the revolution speed was varied to

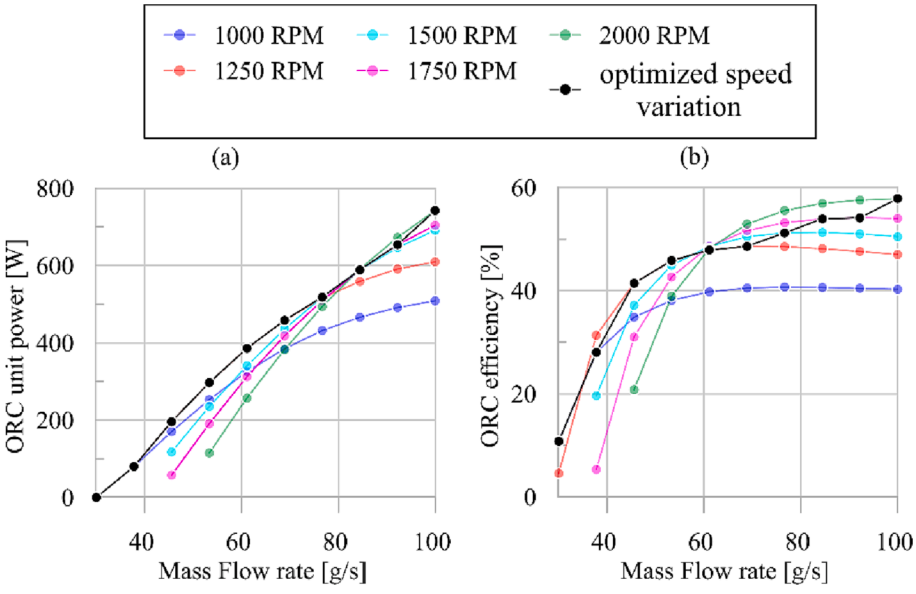

Fig. 9. Expander power (a) and Expander efficiency (b) as a function of R245fa mass flow rate and expander speed.

follows the black path of Fig. 7 are respectively reported.

It can be seen from Fig. 9(a) how the power follows a linear trend from 300 W to 1200 W for the considered mass flow rate excursion. The expander speed regulation should preserve the linear growth of the maximum pressure of the unit with mass flow rate limiting its slope, [29]. In fact, a volumetric expander presents a self-regulation capability even if its speed is not regulated. So, the revolution speed variation ensures that the maximum pressure does not reach too high or too low values for high increase or decrease of mass flow rate entering the machine, respectively.

Concerning the efficiency, Fig. 9(b) shows a flat overall trend being the excursion in the 0.4–0.45 range. So, with a proper revolution speed variation, the efficiency of the machine sees a slight reduction from the design value (0.45).

The expander speed optimization profile also allows to maximize the power of the unit (Fig. 10(a)) and efficiency (Fig. 10(b)) confirming the validity of the expander speed optimization observed in the previous section for a wider mass flow rate range.

In Fig. 10(a) can be seen how a properly change of the speed the unit produces a higher power for each mass flow rate with respect to the case of a fixed speed. The same happens for the ORC efficiency (Fig. 10(b)) and in this case it is important to observe that after 60 g/s, the efficiency reaches a flat trend close to 3%.

Hence, the main limit of the efficiency of the unit is constituted by the high power required by the pump as it usually happens when the power of the unit based on a Rankine or Hirn cycle decreases. This aspect is particularly severe for the condition at hand where the rated power of the expander is limited to value lower than 1 kW.

For this reason and due to the limitation of the hot source, the operating of the expander is higher than that of the whole ORC unit. This means how he same expander can be suitable also for larger scale.

Anyway, it is shown as a wider revolution speed variation ensures to widen the machine and plant operability with respect to the experimental cases. Indeed, reducing the revolution speed at 1000 RPM for a mass flow rate lower than 50 g/s, the unit produces a power up to 300 W with a maximum efficiency of 2.3%. On the other hand, for mass flow rates higher than 80 g/s, at 2000 RPM it is possible to avoid unsuitable maximum pressure ensuring a power production up to 700 W with a maximum plant efficiency of 3%.

4. Discussions

In the present paper it was seen as the adoption of a variable speed sliding rotary vane expander allows to widen the operating flexibility of a solar driven ORC-based power unit. Indeed, it can be seen as varying the expander speed, the expander permeability can be managed to set the desired expander intake pressure can be assured for a given mass flow rate (and consequently pump speed). Consequently, the superheating degree of working fluid at expander inlet can be kept close to design condition (10) °C) for all the experimented test range. Hence, results shows that a control of the ORC unit based on the expander speed regulation is a fast and robust strategies [26].

Concerning the ORC performance they are in line with the literature results about ORC-based unit with the same size. Indeed, A maximum plant efficiency close to 4% is already observed in [21] (4–6%), [38] (3–4%), [37] (4%), [25]. It was found that the main limit of the unit is the higher power as confirmed by the high backwork ratio up to 70% in line with [25].

Besides such parameters there are many others which could be considered (thermal power availability at the hot source in terms of water flow rate from the reservoir or the temperature at evaporator inlet or the availability of solar power). Nevertheless, the main scope of the present study is to evaluate the operability of a small Sliding Rotary Vane Expander which suffers severe off design conditions (low hot source temperature is the most critical aspect). Hence, main parameters characterizing the SVRE operating conditions identified as expander intake pressure, efficiency, power delivered and expander speed were considered being the last one an important degree of freedom for plant management. Indeed, when this parameter is matched with pump speed (WF flow rate) a reliable control strategy allows to limit the maximum pressure of the unit. Such concept was introduced inside the text.

An interesting results of the present research is the variable speed expander present a wide a wider operating range with respect to that of the unit. In fact, the limited thermal power of the hot source and the high power requirement of the pump reduce the mass flow rate range in which the unit can operate (30–100 g/s). Consequently, the present machine properly setting the revolution speed could be suitable for different scale of ORC based power unit.

Concerning the expander performance, they are comparable with results collected on expanders with similar size in literature. In the present work it is found an isentropic efficiency comprised between 40 and 50% similar to what found by [39,40] in which SVRE of a similar

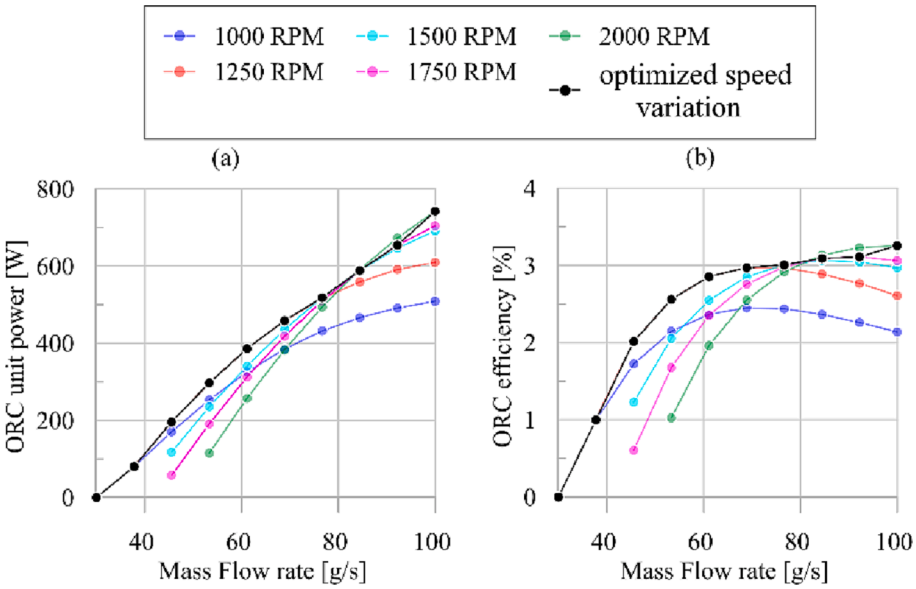

Fig. 10. ORC power (a) and ORC efficiency (b) as a function of R245fa mass flow rate and expander speed.

size were tested.

Scroll expander presents a higher efficiency for the same scale as reported in [41] (50%) and in [42] (70%).

SVRE performance could be enhanced introducing the dual intake technology which allows to reduce the performance gap as observed in [43].

Hence, SVRE allows to widen the solar ORC unit operating range allowing to deal the severe off-design operating conditions taking place for the high variability of the solar source and the demand of DHW. In this sense, an important feature of SVRE is that reducing the expander speed, a proper expander pressure ratio is guaranteed when the working fluid flow rate is reduced due the scarce thermal power availability of the hot source. On the other hand, if the expander speed is increased the expander could elaborate more mass flow rate keeping constant the intake pressure. This feature allows to size the plant not in correspondence of the maximum operating point but for the most probable reducing the risk that the plant is oversized. So, the situation of extra availability of thermal power are fulfilled with the increase of expander speed. A further aspect is the reduction of the mechanical stresses which machine components must face decreasing the expander intake pressure for a given mass flow rate if its rotation increases.

So, the coupling of an ORC-based power unit fed by the hot water inside a reservoir usually present in a conventional flat plate solar collector plant consents a much wider exploitation of the solar energy which irradiates the panels. Thermally discharging the reservoir thanks to the electricity generation allows a continuous solar energy recovery. In fact, in real operating conditions when the reservoir reached the preset temperature level, the solar energy recovery is stopped. Considering that the thermal energy inside the reservoir in domestic applications is usually greater that real use (the system is almost always overdesigned), flat plate solar collectors are simply irradiated losing a potential greater recovery which, on the contrary, is guaranteed by the generating unit. A continuous recovery is enhanced is the unit can properly work as much as the temperature of the hot source (the one inside the reservoir) decreases, The speed of the SVRE is an effective control parameter to insure this. It appears noteworthy to observe that a greater exploitation of the solar energy of a plant already built significantly contributes and appears to be relevant with respect to energy sustainability. This is even more underlined by the fact that the greater exploitation produces electrical energy which has a greater values from a thermodynamic point of view with respect to thermal energy which, anyway, is kept available for users. The electricity stored inside a battery at domestic level contributes to reduce the requests from the grid insuring also an economic saving.

5. Conclusions

In the present paper, the impact of the expander revolution speed variation on a solar micro-cogenerative ORC-based power unit was experimentally and theoretically characterized.

A fully instrumented ORC-based power unit was developed simulating the solar power through two electric resistances heating 135 Liters of water stored in a thermal storage tank. To make the plant more robust to the variation of the operating conditions, a sliding rotary vane expander SVRE was adopted with the possibility to regulate its revolution speed without changing the electrical energy frequency. By varying the revolution speed, in correspondence variations of the WF mass flow rate, ensures to control maximum pressure of the plant, so the expander working conditions. Varying the expander speed, the machine and plant permeability change breaking the linear growth of the maximum pressure. In other words, for a given WF mass flow rate which depends on the thermal recovery at the HRVG, a desired maximum pressure of the plant or a desired expander pressure ratio can be achieved by varying the expander speed which revealed a suitable control variable in accordance with literature.

This was widely demonstrated by the experimental analysis which shows that the slope of the linear growth of the intake pressure with mass flow rate decreases with the WF mass flow rate. This provides also an experimental demonstration of the permeability theory developed by the authors in previous works. Indeed the following experimental evidences was observed:

1. Increasing the expander speed from 1250 RPM up to 1750 RPM, the expander permeability grows from 0.08 kg/(Mpa·s) up to 0.1 kg/(Mpa·s);
2. Increasing the expander speed allows to avoid too high excursion of expander intake pressure thus keeping the expander pressure ratio close to the design value;
3. An optimized speed profile is experimentally derived selecting for each mass flow rate the expander speed allowing to maximize the expander power;
4. It was seen as the optimized speed profile ensures also to optimize the expander efficiency and the ORC plant power and efficiency;

Tanks to the comprehensive validation of the expander model which accounted for the revolution speed, a wider analysis concerning the power producible by the recovery unit was predicted as well as the expected performances of the expander. The model results show:

1. SVRE allows to widen the ORC unit operability over a mass flow rate range comprised between 30 and 100 g/s;
2. Optimized speed curve maintains its validity also for a larger operating range;
3. SVRE presents a higher operating range than the ORC unit due to the lower hot source power and high backwork ratio;
4. The maximum power (800 W) and plant efficiency (3–4%) are limited by the high pump power requirement which represent the most critical element also for the lower expander rated power.

The expander revolution speed variation allows to avoid the ORC plant is over-desinged. Indeed, it can be sized considering the most probable working point and not the one characterized by the maximum power. The expander speed variation allows to set the plant scale according to the operating conditions variations.

CRediT authorship contribution statement

Fabio Fatigati: Conceptualization, Methodology, Investigation, Software, Data curation, Validation, Visualization, Writing – original draft. **Diego Vittorini:** Data curation, Investigation, Methodology, Visualization, Writing – original draft. **Marco Di Bartolomeo:** Visualization, Investigation, Data curation, Writing – original draft. **Roberto Cipollone:** Conceptualization, Methodology, Supervision, Writing – original draft.

Declaration of Competing Interest

The authors declare that they have no known competing financial interests or personal relationships that could have appeared to influence the work reported in this paper.

Data availability

Data will be made available on request.

Acknowledgments

The authors are grateful to SIVAM S.r.l. and Ing. Enea Mattei S.p.A. for the support given during this activity. New subroutines employed in the model were developed in the framework of the European project Development of efficient and environmental friendly LONG distance powertrain for heavy duty trucks and coaches: LONGRUN GRANT

AGREEMENT NUMBER 874972.

References

[1] Ritchie H, Roser M, Rosado P, Energy, Our World Data. (2020). https://ourworldindata.org/energy (accessed September 21, 2022).
[2] IEA, Tracking Buildings 2021, Paris, 2021.
[3] IEA, Gas 2020, n.d. www.iea.org/t&c/.
[4] REN21, Renewables 2018 Global Status Report, n.d. https://www.ren21.net/wp-content/uploads/2019/05/GSR2018_Full-Report_English.pdf (accessed September 21, 2022).
[5] Alemam A, Al-Widyan MI. Technical, economic, and environmental assessment of integrating solar thermal systems in existing district heating systems under Jordanian climatic conditions. J Sustain Dev Energy, Water Environ Syst 2022;10(3):1–16.
[6] Turanjanin V, Bakić V, Jovanović M, Pezo M. Fossil fuels substitution by the solar energy utilization for the hot water production in the heating plant "Cerak" in Belgrade. Int J Hydrogen Energy 2009;34:7075–80. https://doi.org/10.1016/J.IJHYDENE.2008.11.005.
[7] Carotenuto A, Figaj RD, Vanoli L. A novel solar-geothermal district heating, cooling and domestic hot water system: Dynamic simulation and energy-economic analysis. Energy 2017;141:2652–69. https://doi.org/10.1016/J.ENERGY.2017.08.084.
[8] Visa I, Moldovan M, Duta A. Experimental performance assessment of vertically installed solar thermal collectors. J Sustain Dev Energy, Water Environ Syst 2020;8:692–700. https://doi.org/10.13044/j.sdewes.d7.0287.
[9] Shemelin V, Matuska T. Unglazed solar thermal collector for building facades. Energy Rep 2022;8:605–17. https://doi.org/10.1016/J.EGYR.2022.07.075.
[10] Dehghan M, Pfeiffer C. Modelling and control of collecting solar energy for heating houses in Norway. J Sustain Dev Energy, Water Environ Syst 2017;5:359–76. https://doi.org/10.13044/j.sdewes.d5.0147.
[11] Zambrana-Vasquez D, Aranda-Usón A, Zabalza-Bribián I, Jañez A, Llera-Sastresa E, Hernandez P, et al. Environmental assessment of domestic solar hot water systems: a case study in residential and hotel buildings. J Clean Prod 2015;88:29–42. https://doi.org/10.1016/J.JCLEPRO.2014.06.035.
[12] Villasmil W, Troxler M, Hendry R, Schuetz P, Worlitschek J. Control strategies of solar heating systems coupled with seasonal thermal energy storage in self-sufficient buildings. J Energy Storage 2021;42:103069. https://doi.org/10.1016/J.EST.2021.103069.
[13] Quintana HJ, Kummert M. Optimized control strategies for solar district heating systems. J Build Perform Simul 2015;8:79–96. https://doi.org/10.1080/19401493.2013.876448.
[14] Li X, Wang Z, Li J, Yang M, Yuan G, Bai Y, et al. Comparison of control strategies for a solar heating system with underground pit seasonal storage in the non-heating season. J Energy Storage 2019;26:100963. https://doi.org/10.1016/J.EST.2019.100963.
[15] Borsukiewicz-Gozdur A, Klonowicz P, Kròl D, Wiśniewski S, Zwarycz-Makles K. Techno-economic analysis of CHP system supplied by waste forest biomass. Waste Manag Res 2015;33(8):748–54. https://doi.org/10.1177/0734242X15590472.
[16] Chacartegui R, Muñoz de Escalona J, Becerra JA, Fernández A, Sánchez D. Potential of ORC systems to retrofit CHP plants in wastewater treatment stations. J Sustain Dev Energy, Water Environ Syst 2013;1:352–74. https://doi.org/10.13044/j.sdewes.2013.01.0027.
[17] Guzović Z, Rašković P, Blatarić Z. The comparison of a basic and a dual-pressure ORC (Organic Rankine Cycle): Geothermal Power Plant Velika Ciglena case study. Energy 2014;76:175–86. https://doi.org/10.1016/J.ENERGY.2014.06.005.
[18] Cipollone R, Di Battista D, Bettoja F. Performances of an ORC power unit for waste heat recovery on heavy duty engine. Energy Procedia 2017;129:770–7. https://doi.org/10.1016/j.egypro.2017.09.132.
[19] Hossin K, Mahkamov K, Belgasim B. Thermodynamic analysis and sizing of a small scale solar thermal power system based on organic rankine cycle. J Sustain Dev Energy, Water Environ Syst 2020;8:493–506. https://doi.org/10.13044/j.sdewes.d7.0294.
[20] Gilani HA, Hoseinzadeh S, Esmaeilion F, Memon S, Garcia DA, Assad MEH. A solar thermal driven ORC-VFR system employed in subtropical Mediterranean climatic building. Energy 2022;250:123819. https://doi.org/10.1016/J.ENERGY.2022.123819.
[21] García-Domínguez J, Blanco-Marigorta AM, Daniel Marcos J. Analysis of a solar driven ORC-absorption based CCHP system from a novel exergy approach. Energy Convers Manage: X 2023;19:100402. https://doi.org/10.1016/j.ecmx.2023.100402. ISSN 2590-1745.
[22] Rodriguez-Pastor DA, Becerra JA, Chacartegui R. Adaptation of residential solar systems for domestic hot water (DHW) to hybrid organic Rankine Cycle (ORC) distributed generation. Energy 2023;263(Part D):125901. https://doi.org/10.1016/j.energy.2022.125901. ISSN 0360-5442.
[23] Haoshui Yu, Helland Henrik, Xingji Yu, Gundersen Truls, Sin Gürkan. Optimal design and operation of an Organic Rankine Cycle (ORC) system driven by solar energy with sensible thermal energy storage. Energy Conversion and Management 2021;244:114494. https://doi.org/10.1016/j.enconman.2021.114494. ISSN 0196-8904.
[24] Roumpedakis TC, Loumpardis G, Monokrousou E, Braimakis K, Charalampidis A, Karellas S. Exergetic and economic analysis of a solar driven small scale ORC. Renew Energy 2020;157:1008–24. https://doi.org/10.1016/J.RENENE.2020.05.016.
[25] Ancona MA, Bianchi M, Branchini L, De Pascale A, Melino F, Peretto A, et al. Solar driven micro-ORC system assessment for residential application. Renew Energy 2022;195:167–81. https://doi.org/10.1016/J.RENENE.2022.06.007.
[26] Eyerer S, Dawo F, Schifflechner C, Niederdränk A, Spliethoff H, Wieland C. Experimental evaluation of an ORC-CHP architecture based on regenerative preheating for geothermal applications. Appl Energy 2022;315:119057.
[27] Dickes R, Dumont O, Lemort V. Experimental assessment of the fluid charge distribution in an organic Rankine cycle (ORC) power system. Appl Therm Eng 2020;179:115689. https://doi.org/10.1016/j.applthermaleng.2020.115689. ISSN 1359-4311.
[28] Fatigati F, Di Battista D, Cipollone R. Permeability effects assessment on recovery performances of small-scale ORC plant. Appl Therm Eng 2021;196:117331. https://doi.org/10.1016/j.applthermaleng.2021.117331.
[29] Fatigati F, Di Bartolomeo M, Di Battista D, Cipollone R. Model based control of the inlet pressure of a sliding vane rotary expander operating in an ORC-based power unit. Appl Therm Eng 2021;193:117032. https://doi.org/10.1016/j.applthermaleng.2021.117032.
[30] Pethurajan V, Sivan S, Joy GC. Issues, comparisons, turbine selections and applications – An overview in organic Rankine cycle. Energy Convers Manag 2018;166:474–88. https://doi.org/10.1016/j.enconman.2018.04.058.
[31] Klun M, Guzović Z, Rašković P. Innovative small axial multistage turbine with partial admission for bottoming ORC. Energy Rep 2021;7:9069–93. https://doi.org/10.1016/J.EGYR.2021.11.229.
[32] Deligant M, Sauret E, Danel Q, Bakir F. Performance assessment of a standard radial turbine as turbo expander for an adapted solar concentration ORC. Renew Energy 2020;147:2833–41.
[33] Quoilin S, Van Den Broek M, Declaye S, Dewallef P, Lemort V. Techno-economic survey of Organic Rankine Cycle (ORC) systems. Renew Sustain Energy Rev 2013;22:168–86. https://doi.org/10.1016/J.RSER.2013.01.028.
[34] Ziviani D, Suman A, Lecompte S, De Paepe M, Van Den Broek M, Spina PR, et al. Comparison of a single-screw and a scroll expander under part-load conditions for low-grade heat recovery ORC systems. Energy Procedia 2014;61:117–20. https://doi.org/10.1016/j.egypro.2014.11.920.
[35] Fatigati F, Vittorini D, Coletta A, Cipollone R. Assessment of the differential impact of scroll and sliding vane rotary expander permeability on the energy performance of a small-scale solar-ORC unit. Energy Convers Manag 2022;269:116169. https://doi.org/10.1016/J.ENCONMAN.2022.116169.
[36] Ottaviano Saverio, Poletto Chiara, Ancona Maria Alessandra, Melino Francesco. Experimental investigation on micro-ORC system operating with partial evaporation and two–phase expansion. Energy Convers Manage 2022;274:116415. https://doi.org/10.1016/j.enconman.2022.116415. ISSN 0196-8904.
[37] Unamba CK, Sapin P, Li X, Song J, Wang K, Shu G, et al. Operational optimisation of a non-recuperative 1-kWe organic Rankine cycle (ORC) engine prototype. Appl Sci 2019;9:1–19. https://doi.org/10.3390/app9153024.
[38] Zhang Y-F, Li M-J, Ren X, Duan X-Y, Chia-Jung Wu, Xi H, et al. Effect of heat source supplies on system behaviors of ORCs with different capacities: An experimental comparison between the 3 kW and 10 kW unit. Energy 2022:124267. https://doi.org/10.1016/j.energy.2022.124267. ISSN 0360-5442.
[39] Mascuch J, Novotny V, Vodicka V, Spale J, Zeleny Z. Experimental development of a kilowatt-scale biomass fired micro – CHP unit based on ORC with rotary vane expander. Renew Energy 2020;147:2882–95.
[40] Naseri Ali, Moradi Ramin, Norris Stuart, Subiantoro Alison. Experimental investigation of a revolving vane expander in a micro-scale organic Rankine cycle system for low-grade waste heat recovery. Energy 2022;253:124174. https://doi.org/10.1016/j.energy.2022.124174. ISSN 0360-5442.
[41] Ziviani D, James NA, Accorsi FA, Braun JE, Groll EA. Experimental and numerical analyses of a 5 kWe oil-free open-drive scroll expander for small-scale organic Rankine cycle (ORC) applications. Appl Energy 2018;230:1140–56. https://doi.org/10.1016/j.apenergy.2018.09.025. ISSN 0306-2619.
[42] Declaye S, Quoilin S, Guillaume L, Lemort V. Experimental study on an open-drive scroll expander integrated into an ORC (Organic Rankine Cycle) system with R245fa as working fluid. Energy 2013;55:173–83. https://doi.org/10.1016/j.energy.2013.04.003. ISSN 0360-5442.
[43] Fatigati F, Di Giovine G, Cipollone R. Feasibility assessment of a dual intake-port scroll expander operating in an ORC-based power unit. Energies 2022;15:770. https://doi.org/10.3390/en15030770.